

# Screening of transition and post-transition metals to incorporate into copper oxide and copper bismuth oxide for photoelectrochemical hydrogen evolution†

Cite this: *Phys. Chem. Chem. Phys.*, 2013, **15**, 4554

Sean P. Berglund,<sup>a</sup> Heung Chan Lee,<sup>b</sup> Paul D. Núñez,<sup>a</sup> Allen J. Bard<sup>b</sup> and C. Buddie Mullins<sup>\*ab</sup>

A new dispenser and scanner system is used to create and screen Bi–M–Cu oxide arrays for cathodic photoactivity, where M represents 1 of 22 different transition and post-transition metals. Over 3000 unique Bi : M : Cu atomic ratios are screened. Of the 22 metals tested, 10 show a M–Cu oxide with higher photoactivity than CuO and 10 show a Bi–M–Cu oxide with higher photoactivity than CuBi<sub>2</sub>O<sub>4</sub>. Cd, Zn, Sn, and Co produce the most photoactive M–Cu oxides, all showing a 200–300% improvement in photocurrent over CuO. Ag, Cd, and Zn produce the highest photoactivity Bi–M–Cu oxides with a 200–400% improvement over CuBi<sub>2</sub>O<sub>4</sub>. Most notable is a Bi–Ag–Cu oxide (Bi : Ag : Cu atomic ratio of 22 : 3 : 11) which shows 4 times higher photocurrent than CuBi<sub>2</sub>O<sub>4</sub>. This material is capable of evolving hydrogen under illumination in neutral electrolyte solutions at 0.6 V vs. RHE when Pt is added to the surface as an electrocatalyst.

Received 29th October 2012,  
Accepted 7th February 2013

DOI: 10.1039/c3cp50540e

[www.rsc.org/pccp](http://www.rsc.org/pccp)

## 1. Introduction

In theory, efficient photoelectrochemical (PEC) water splitting to produce hydrogen and oxygen by solar irradiation of a semiconductor material in water is an ideal method for renewable energy production. When it is produced by solar energy hydrogen is a carbon neutral fuel with no harmful combustion products. Less than 1% of the sun's incident power and only about  $2 \times 10^{-6}$ % of the earth's ocean water is required to produce enough hydrogen to meet the current world power demand using solar energy.<sup>1</sup> In practice, economical hydrogen production by PEC water splitting remains a tremendous challenge. We have not yet discovered a semiconductor material that demonstrates high solar-to-hydrogen (STH) efficiency, remains stable in electrolyte indefinitely, and is composed of abundant elements. For this reason the identification of new materials is crucial to the advancement of PEC water splitting. The first economical PEC

water splitting system will likely be a multi-component device, such as a tandem PEC cell which utilizes both a p-type photocathode and n-type photoanode, since multi-component devices allow for higher theoretical efficiencies.<sup>2–4</sup>

Several p-type semiconductor materials with reasonable STH efficiencies (>5%) have already been discovered. In 1982 p-InP (Rh–H alloy) and p-InP (Re–H alloy) photocathodes were tested for the photo-reduction of hydrogen with solar-to-chemical efficiencies calculated at 13.3% and 11.4%, respectively.<sup>5</sup> p-Si, when coated with electrocatalysts such as discontinuous Pt islands, can also achieve relatively high efficiencies for photo-reduction reactions.<sup>6–8</sup> Recently, attempts have been made to improve p-Si further by altering the nanostructure. For example nanoporous black silicon photocathodes showed IPCE values around 90% in 0.5 M H<sub>2</sub>SO<sub>4</sub> at –1.0 V vs. Ag/AgCl (–0.8 V vs. RHE) for 500 to 700 nm light.<sup>9</sup> Thin film photovoltaic materials such as CuGaSe<sub>2</sub> (CGS) and Cu(In,Ga)Se<sub>2</sub> (CIGS) have also shown reasonably high efficiencies when used as photocathodes. CuGaSe<sub>2</sub> achieved a photocurrent of 10.5 mA cm<sup>–2</sup> in 0.5 M H<sub>2</sub>SO<sub>4</sub> at –0.9 V vs. SCE (–0.7 V vs. RHE) under AM1.5 illumination.<sup>10</sup> Cu(In,Ga)Se<sub>2</sub> with Pt as an electrocatalyst achieved a quantum efficiency of 19% at –0.24 V vs. RHE.<sup>11</sup> There is one major shortcoming with all of the previously mentioned p-type materials. They all require a large negative bias to reach the limiting photocurrent. In some cases the potential applied is even more negative than the thermodynamic

<sup>a</sup> Department of Chemical Engineering, Center for Electrochemistry, Texas Materials Institute, and Center for Nano- and Molecular Science, University of Texas at Austin, 1 University Station C0400, Austin, TX 78712, USA

<sup>b</sup> Department of Chemistry and Biochemistry, Center for Electrochemistry, Texas Materials Institute, and Center for Nano- and Molecular Science, University of Texas at Austin, 1 University Station C0400, Austin, TX 78712, USA.  
E-mail: [mullins@che.utexas.edu](mailto:mullins@che.utexas.edu)

† Electronic supplementary information (ESI) available. See DOI: 10.1039/c3cp50540e

$H^+$  reduction potential, which defeats the purpose of using light to drive the hydrogen evolution reaction (HER). The addition of precious metals such as Pt helps, but the maximum cathodic photocurrent is still not achieved until potentials more negative than 0.4 V vs. RHE. This makes these materials less useful for a tandem PEC device because the overlap in photocurrent of both the photocathode and photoanode at a single potential determines the operating current of such a device.<sup>4</sup>

Two alternative p-type semiconductor materials that have much more positive cathodic photocurrent onset potentials are CuO and  $CuBi_2O_4$ . CuO is reported to have a band gap energy between 1.35 and 1.7 eV.<sup>12–16</sup> It has been shown to have an onset potential near 0.28 V vs. SCE in 0.25  $Na_2SO_4$  at pH 6.72 (0.9 V vs. RHE) and is capable of reaching photocurrents on the order of 1  $mA\ cm^{-2}$ .<sup>17</sup> Unfortunately, the electrochemical potential for the reduction of CuO to  $Cu_2O$  in aqueous solutions is less negative than both the potential for proton reduction and the conduction band of CuO, which makes the material highly unstable in aqueous electrolytes under illumination.<sup>17,18</sup> Moreover, the potential for reducing  $Cu_2O$  to pure Cu is more positive than both the potential for proton reduction and the conduction band of  $Cu_2O$  so it is also unstable.<sup>18</sup> On the other hand,  $CuBi_2O_4$  has been reported to be stable as an electrode.<sup>19</sup> It has a light absorption threshold between 1.55 and 1.8 eV and a cathodic photocurrent onset between 1.0 and 1.1 V vs. RHE.<sup>19,20</sup> However, the photo-conversion efficiency of  $CuBi_2O_4$  appears to be low and it may not be stable for all synthesis techniques.<sup>20</sup> If the stability of CuO and the efficiency of  $CuBi_2O_4$  can be improved then these materials show promise for use as photocathodes in a tandem PEC device. One method for improving the stability and efficiency of materials for PEC water splitting is through incorporation of additional elements or doping.<sup>21–24</sup> This paper describes a combinatorial chemistry study of transition and post-transition metals for incorporation into CuO and  $CuBi_2O_4$  to improve the PEC performance for photo-reduction reactions.

Combinatorial chemistry is a methodology that involves rapid synthesis of a large number of related molecules or materials, which can be screened for a specific application. It is often referred to as high-throughput screening. Pioneering work in combinatorial chemistry began in the 1960's with automated synthesis of peptides and continued research in the field of drug discovery.<sup>25,26</sup> Combinatorial chemistry wasn't applied to materials research until the 1990's, when it was used to investigate large magnetoresistance materials, luminescent materials, heterogeneous catalysts, and polymer thin-films.<sup>27–32</sup> Even more recently, combinatorial techniques have been applied to the field of photocatalysis and photo-electrochemistry. Lettmann *et al.* were the first to report a combinatorial technique for investigating photocatalysts in 2001.<sup>33</sup> They used a sol-gel method to dope  $TiO_2$ ,  $SnO_2$ , and  $WO_3$  with various metal salts and assessed the photocatalytic activity for water purification by measuring the degradation of a model pollutant (4-chlorophenol) under illumination. Since then other research groups have demonstrated a variety of techniques for high-throughput screening of photocatalytic materials. Nakayama *et al.* used molecular beam epitaxy (MBE) combined with a mask to

deposit  $TiO_2$  films doped with cobalt.<sup>34</sup> The photocatalytic activity was assessed by reducing ferric ions and oxidizing water resulting in an increase in protons that were detected by 2-dimensional pH measurements.<sup>34</sup> Jaramillo *et al.* used automated electrochemical deposition to create libraries of mesoporous  $ZnO$  and varying composition  $Zn_{1-x}Co_xO$  thin films, which were measured using a photo-electrochemical cell with a moveable probe.<sup>35,36</sup> Goldsmith *et al.*, synthesized heteroleptic iridium complexes using a variety of precursor solutions.<sup>37</sup> The complexes were placed in vials containing triethanolamine (TEOA) as the sacrificial reductant and illuminated while measuring  $H_2$  production with a hydrogen sensor. Dai *et al.*, mixed a variety of metal nitrate solutions with a  $TiCl_4$  precursor solution and silica to synthesize doped  $TiO_2$  on  $SiO_2$  supports.<sup>38</sup> They reacted 1,6-hexamethylenediamine with fluorescamine, measured the fluorescence, and correlated it to the photocatalytic activity of each material. Arai *et al.* developed an automated system for dispensing precursor solutions onto FTO glass for material synthesis by metal organic decomposition (MOD).<sup>19</sup> Photoactivity was tested in a 3-electrode PEC. Seyler *et al.* used the sol-gel method to make photocatalyst materials and measured the hydrogen production under illumination using gas chromatography.<sup>39</sup> Other researchers have used inkjet printers to synthesize mixed-metal oxide arrays on FTO followed by PEC testing in 2 and 3-electrode PEC cells.<sup>23,40,41</sup> Lee *et al.* dispensed metal nitrate precursor solutions with a single piezoelectric dispenser onto FTO.<sup>42</sup> The FTO was annealed creating mixed metal oxide arrays, which were scanned by placing them in a 3-electrode cell and using a scanning electrochemical microscope (SECM) to raster a fiber optic tip across the surface while measuring the photocurrent. This approach has been used successfully to identify several high photoactivity n-type materials such as Sn/Ti doped  $Fe_2O_3$ , W doped  $BiVO_4$  and Mo/W doped  $BiVO_4$  for use as photoanodes.<sup>43–47</sup> We have taken a similar approach and developed a new array dispenser and scanner system capable of screening arrays with a larger number of chemical components at a much faster rate. More details of the array scanner and dispenser system are given in the Experimental section below.

## 2. Experimental

### 2.1 Array dispenser and scanner system

Fig. 1 shows a schematic of the array dispenser that we developed and used for this study. The array dispenser consisted of a printhead assembly (MicroFab, PH046H-AT), which held up to four 2 ml fluid reservoirs and four piezoelectric microdispensing devices (MicroFab, MJ-AT-01-80). The pressure in each reservoir was varied by a pneumatic controller (MicroFab, CP-PT4), which was connected to a vacuum/pressure pump (Thermo Scientific, 420-1901). Each reservoir contained a precursor solution that was fed to one of the four microdispensing devices. The printhead assembly was mounted on a 3-dimensional positioner (CH Instruments). The positioner and microdispensing devices were connected to a 3-dimensional positioner controller/piezo jet device controller (CH Instruments, 1560A), which was connected

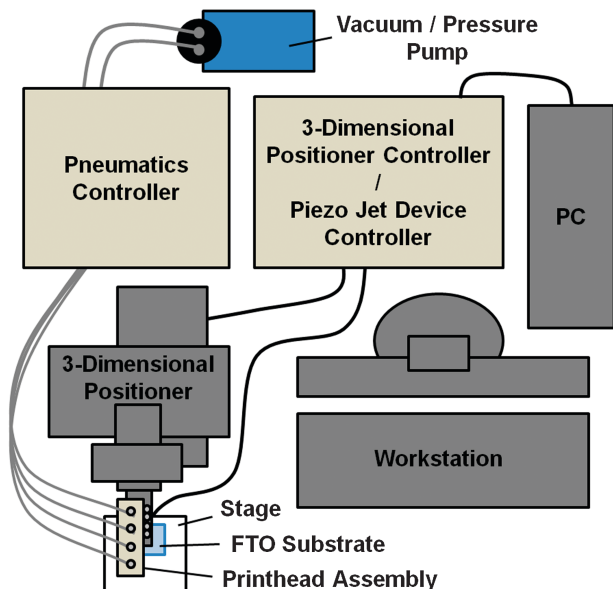


Fig. 1 Schematic of array dispenser.

to a standard PC and user workstation. CH Instruments software was used to control the array dispenser system. Each microdispensing device had an orifice diameter of 80  $\mu\text{m}$  and was capable of dispensing individual drops in the range of 150 to 350 pL depending on the solvent used for the precursor solution and the voltage pulse applied. Based on measurements of the mass dispensed we estimate that the drop size varied by approximately  $\pm 14\%$  from device to device when using the same voltage pulse. To create an array, varying amounts of each precursor solution was dispensed in a pattern on a hydrophobic fluorine doped tin oxide (FTO) substrate. To make the FTO substrates hydrophobic they were cleaned and sonicated in reagent alcohol (PHARMCO-AAPER, 99.5%), soaked in 3:50 dichlorodimethylsilane (ACROS, 99+%): *n*-hexane (ACROS, 95%), rinsed in *n*-hexane, and then heated at 60  $^{\circ}\text{C}$  in a vacuum oven for 1–2 hours. Arrays were dispensed onto the cleaned FTO substrates, which were placed in a vacuum oven at 80  $^{\circ}\text{C}$  for 15 minutes to flatten the spots for adherence and then annealed at 500  $^{\circ}\text{C}$  for 2 hours to form mixed metal oxides.

Fig. 2 shows a schematic of the array scanner that we developed. It consisted of a Teflon 3-electrode electrochemical cell with the array in the bottom as the working electrode (WE), a platinum wire (Alfa Aesar, 0.6 mm diameter, 99.95% purity) counter electrode (CE), and a Ag/AgCl (CH Instruments, CHI111) reference electrode (RE). The electrochemical cell was filled with an electrolyte and connected to an electrochemical analyzer (CH Instruments, CHI601D). A polished optical fiber with a 400  $\mu\text{m}$  diameter core (Thorlabs, BFH48-400) was used to illuminate the array during scans. One end of the fiber was illuminated with a 100 W xenon lamp (Newport, Model 66452) with a filter (Newport, Schott KG3) and the fiber tip at the opposite end was held in electrolyte approximately 150  $\mu\text{m}$  above the array by a 3-dimensional positioner (CH instruments). A custom LabVIEW program was used to control both the electrochemical

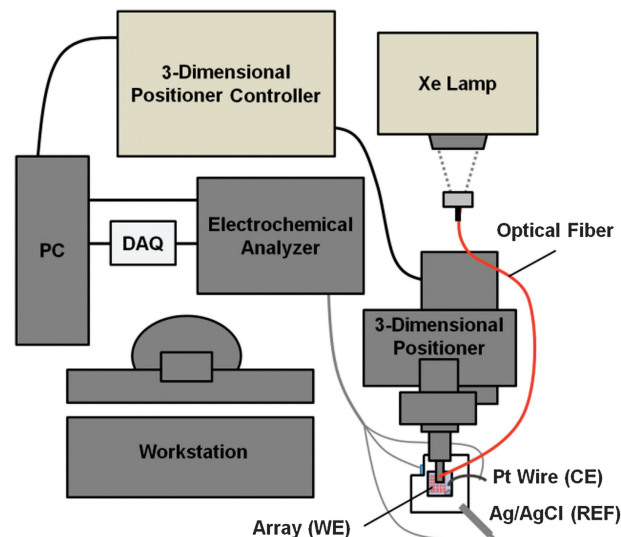


Fig. 2 Schematic of array scanner.

analyzer and 3-dimensional positioner. During a scan the electrochemical cell was held at a constant potential and the optical fiber tip was rastered over the array at a rate of 250–500  $\mu\text{m s}^{-1}$  while the current was recorded through a data acquisition (DAQ) board (National Instruments, USB-6009).

## 2.2 Array synthesis and measurement parameters

For this study, 22 different metals (Ag, Cd, Zn, Al, Ga, In, La, Sc, Y, Sn, Ti, Zr, Nb, Ta, V, Cr, Mo, W, Mn, Co, Fe, Ni) were dispensed along with Bi and Cu onto arrays. Each precursor solution consisted of a metal ion dissolved at a concentration of 0.15 M in ethylene glycol. Metal nitrates ( $\text{AgNO}_3$ ,  $\text{Cu}(\text{NO}_3)_2 \cdot x\text{H}_2\text{O}$ ,  $\text{Cd}(\text{NO}_3)_2 \cdot 4\text{H}_2\text{O}$ ,  $\text{Zn}(\text{NO}_3)_2 \cdot x\text{H}_2\text{O}$ ,  $\text{Al}(\text{NO}_3)_3 \cdot x\text{H}_2\text{O}$ ,  $\text{Ga}(\text{NO}_3)_3 \cdot x\text{H}_2\text{O}$ ,  $\text{In}(\text{NO}_3)_3 \cdot x\text{H}_2\text{O}$ ,  $\text{La}(\text{NO}_3)_3 \cdot 6\text{H}_2\text{O}$ ,  $\text{Ga}(\text{NO}_3)_3 \cdot x\text{H}_2\text{O}$ ,  $\text{Y}(\text{NO}_3)_3 \cdot x\text{H}_2\text{O}$ ,  $\text{Bi}(\text{NO}_3)_3 \cdot x\text{H}_2\text{O}$ ,  $\text{Cr}(\text{NO}_3)_3 \cdot x\text{H}_2\text{O}$ ,  $\text{Mn}(\text{NO}_3)_2 \cdot x\text{H}_2\text{O}$ ,  $\text{Co}(\text{NO}_3)_2 \cdot 6\text{H}_2\text{O}$ ,  $\text{Fe}(\text{NO}_3)_3 \cdot 9\text{H}_2\text{O}$ ,  $\text{N}_2\text{NiO}_6 \cdot 6\text{H}_2\text{O}$ ) were dissolved in ethylene glycol (ACROS, 99+%). Metal chlorides ( $\text{SnCl}_4 \cdot x\text{H}_2\text{O}$ ,  $\text{TiCl}_4$ ,  $\text{ZrCl}_4$ ,  $\text{NbCl}_5$ ,  $\text{TaCl}_5$ ,  $\text{VCl}_3$ ) were dissolved in anhydrous ethylene glycol (Sigma-Aldrich, 99.8%) inside a glove box.  $(\text{NH}_4)_6\text{Mo}_7\text{O}_{24} \cdot 4\text{H}_2\text{O}$  and  $(\text{NH}_4)_{10}\text{W}_{12}\text{O}_{41} \cdot 5\text{H}_2\text{O}$  were dissolved in ethylene glycol (Fischer, certified). A complete list of chemical suppliers and purities is included in the ESI.†

For the initial screening we dispensed and scanned 22 different  $19 \times 19$  Bi–M–Cu arrays on 3 cm  $\times$  3 cm FTO substrates (Hartford Glass, TEC15, 2.3 mm thick) according to the pattern shown in Fig. 3. Dispensing was done with a spot spacing of 550–650  $\mu\text{m}$ , pulse amplitude of 90 V, pulse width of 25  $\mu\text{s}$ , and pulse period of 10 ms. Each spot consisted of a total of 18 drops (18 voltage pulses) with varying amounts from each precursor solution allowing concentration increments of 5.6%. The arrays consisted of a repeat pattern (symmetric across the diagonal) so that the 153 unique Bi:M:Cu atomic ratios could be scanned twice with a single array. The corners were pure components (18 drops of a single precursor solution) and four pure Cu spots were placed in the upper/lower left corner as

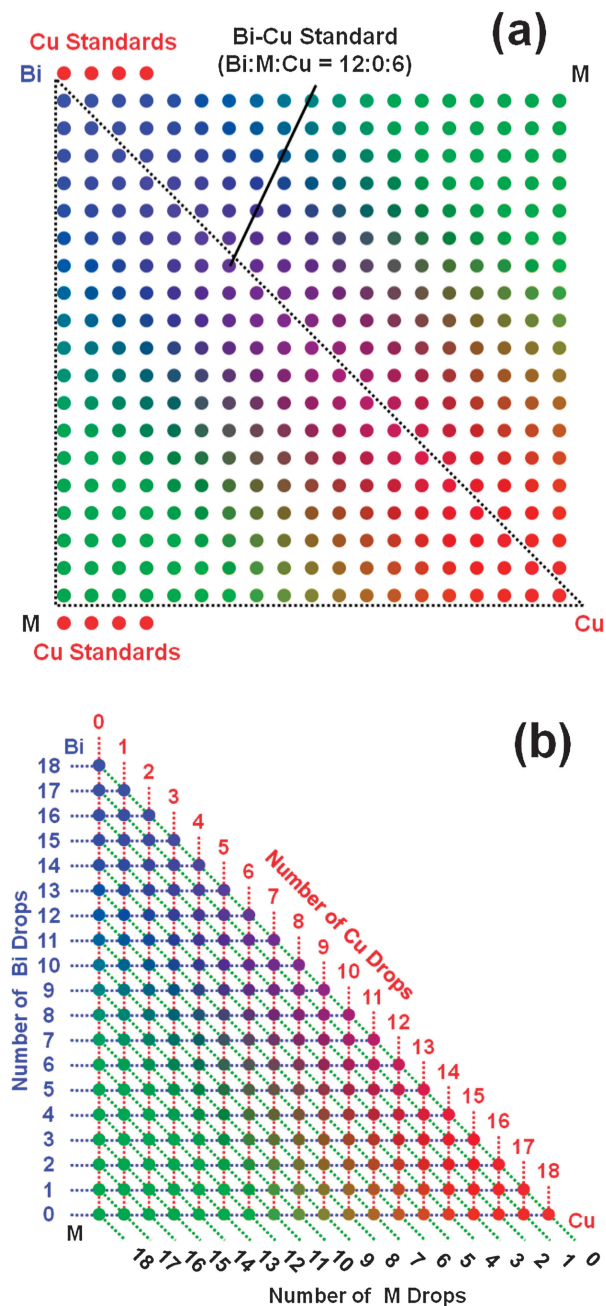


**Fig. 3** Pattern used for the initial  $19 \times 19$  Bi-M-Cu arrays. Bi and Cu were kept constant while M represents one of the 22 transition or post-transition metals. (a) Shows the entire pattern with two repeat triangles symmetric about the diagonal. (b) Indicates the number of drops from each component in the triangle adding up to 18 drops per spot.

standards (Cu oxide standard). The spot with an atomic ratio of Bi : M : Cu = 12 : 0 : 6 in the diagonal of the array was also used as a standard (Bi-Cu oxide standard). With the above settings it took 16 minutes to complete a  $19 \times 19$  Bi-M-Cu array (6786 dispensed drops).

Initial scans were done at a constant potential of  $-0.1$  V vs. Ag/AgCl in  $0.1$  M  $\text{Na}_2\text{SO}_4$  (pH 5.9) with an optical fiber tip scan rate of  $300\text{--}500$   $\mu\text{m s}^{-1}$  without purging the electrolyte with nitrogen. After the initial  $19 \times 19$  Bi-M-Cu array screening we

designed fine increment Bi-M-Cu arrays for the metals that showed acceptable photo-activity relative to the Cu oxide and Bi-Cu oxide standards. Example patterns are shown later in the Results and Discussion. These arrays were dispensed onto  $1.5$  cm  $\times$   $1.5$  cm substrates using a spot spacing of  $1000$   $\mu\text{m}$ , pulse amplitude of  $90$  V, pulse width of  $25$   $\mu\text{s}$ , and pulse period of  $10$  ms. Each spot consisted of a total of  $36$  drops for concentration increments of  $2.78\%$ . Before each fine increment scan the electrolyte was purged for  $15$  minutes with nitrogen (Matheson). Next the electrochemical cell was covered with a silicone elastomer tent and nitrogen was allowed to continuously flow through the tent over the electrolyte. These scans were done at constant potential of  $-0.1$  V vs. Ag/AgCl in  $0.1$  M  $\text{Na}_2\text{SO}_4$  (pH 5.9) with an optical fiber tip scan rate of  $250$   $\mu\text{m s}^{-1}$ .

### 2.3 Materials scale-up and characterization

After completing the array scans the most photo-active Bi : M : Cu atomic ratios were used to make scaled-up films for materials characterization and PEC testing. Pre-cursor solutions were mixed in the desired Bi : M : Cu atomic ratios and diluted to  $30$  mM. Next  $150$   $\mu\text{L}$  of the  $30$  mM pre-mixed solutions were drop-cast onto  $1.5 \times 1.5$  cm substrates that had been cleaned and sonicated with reagent alcohol (PHARMCO-AAPER, 99.5%). The drop-cast films were dried in air at  $120$   $^\circ\text{C}$  for  $1$  hour and then annealed in air at  $500$   $^\circ\text{C}$  for  $2$  hours. PEC measurements of the scaled-up films were done using a 3-electrode PEC cell, electrochemical workstation/analyzer (CH Instruments 660D), and a full spectrum solar simulator (Newport, Model 9600,  $150$  W xenon lamp) with an AM 1.5 filter (Newport). The film was the WE, a Pt wire (Alfa Aesar,  $1$  mm diameter, 99.95%) was the CE, and the RE was a Ag/AgCl electrode (CH Instruments, CH111). Electrolyte solutions were prepared using  $\text{Na}_2\text{SO}_4$ , sodium phosphate monobasic monohydrate, sodium phosphate dibasic anhydrous (Fisher), and de-mineralized water. Non-aqueous solutions containing NaI (Fisher) and  $\text{I}_2$  (Fisher, crystalline, 99.99+%) in acetonitrile (Fisher, ACS) were also prepared. Potentials were converted to reversible hydrogen electrode (RHE) and normal hydrogen electrode (NHE) for aqueous and non-aqueous solutions, respectively. X-ray diffraction (XRD) measurements were taken on a Bruker-Nonius D8 diffractometer. The Cu  $K\alpha$  radiation source was operated at  $40$  kV and  $40$  mA and measurements were carried out in the  $\theta/2\theta$  mode with an incident angle of  $1^\circ$ . UV-vis transmission measurements were done on a Cary 5000 spectrophotometer. Scanning electron microscope (SEM) images were acquired using a Zeiss Supra 40 VP SEM. Energy dispersive X-ray spectroscopy (EDS) was performed using a Quanta FEG 650 SEM with a Bruker XFlash 5010 EDS detector. X-ray photoelectron spectroscopy (XPS) measurements were performed on a Kratos AXIS Ultra DLD spectrometer with Mg  $K\alpha$  radiation. Hydrogen measurements were done using a 3-electrode cell with the film as the WE in a sealed compartment and an evacuated port for gas collection. Prior to measurements the cell was purged with Ar (PRAXAIR). The cell was controlled using an electrochemical analyzer (CH Instruments Model 630) and illuminated with a  $100$  W xenon lamp (Newport, Model 66452). Gas samples were

collected using a syringe and immediately injected into a gas chromatograph (GC) (SHIMADZU, CG-2014). Pt was deposited onto the surface of some films as an electrocatalyst. This was done by holding the films in 10 mM  $\text{H}_2\text{PtCl}_6 \cdot 6\text{H}_2\text{O}$  (Alfa Aesar, 99.95%) and 0.1 M phosphate buffer (pH 6.8) at 0.0 V vs. Ag/AgCl until a total charge of 10  $\text{mC cm}^{-2}$  had passed.

### 3. Results and discussion

#### 3.1 Photoactive M–Cu oxides and Bi–M–Cu oxides

From the array scans we found that 10 of the 22 transition and post-transition metals (M) formed a M–Cu oxide compound with higher photocurrent than the Cu oxide standard. For each M we determined the most photoactive M:Cu atomic ratio by averaging the results from three to six different fine increment arrays (2.78% concentration increments). Fig. 4 shows a Pareto plot of the most photoactive M:Cu atomic ratios for each M. Photocurrent percent difference values were calculated from the M–Cu oxide and the Cu oxide standard on a single array. In Fig. 4 each point is the average of at least three different arrays while the vertical bars are the minimum and maximum.

To our knowledge this is the first direct comparison of these M–Cu oxide compounds for PEC performance using a single measurement apparatus. In the literature few reports of Cu based ternary oxide materials for photo-reduction reactions exist. Trari *et al.* demonstrated  $\text{H}_2$  evolution from illumination of  $\text{CuYO}_2$  in electrolyte solutions containing  $\text{S}^{2-}$  or  $\text{SO}_3^{2-}$  species, but did not compare  $\text{CuYO}_2$  with other Cu oxide compounds.<sup>48</sup> Saadi *et al.* compared  $\text{H}_2$  evolution from p-type spinel materials of the form  $\text{CuM}_2\text{O}_4$  (M = Al, Cr, Mn, Fe and Co) in 0.025 M  $\text{S}^{2-}$ /1 M KOH and found that  $\text{CuCo}_2\text{O}_4$  was the most photoactive of these materials.<sup>49</sup> Mor *et al.* fabricated CuO rich p-type Cu–Ti–O nanotubes as the photocathode material in a photoelectrochemical diode, but they did not investigate different Ti:Cu ratios or incorporation of other metals besides Ti.<sup>50</sup>

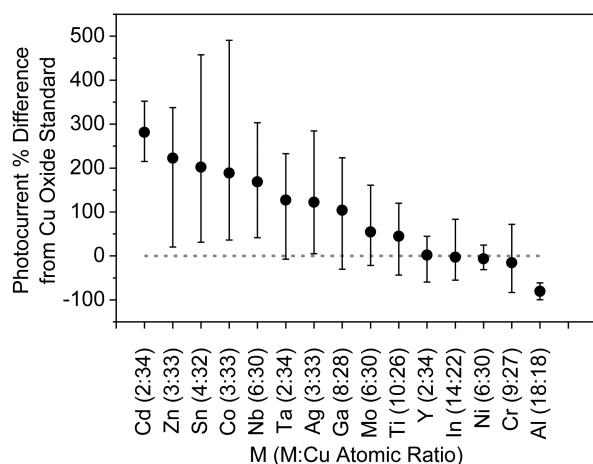


**Fig. 4** Pareto plot of the percent difference in photocurrent of the M–Cu oxide compounds from the Cu oxide standard. Each point is the average of at least three arrays while the vertical bars are the maximum and minimum. Arrays were scanned in 0.1 M  $\text{Na}_2\text{SO}_4$  (pH 5.9) at a potential of  $-0.1$  V vs. Ag/AgCl (0.45 V vs. RHE).

From our results we found that the most photoactive M–Cu oxide materials were composed primarily of Cu (at least 72.2% Cu metals basis). The five most effective metals (Cd, Zn, Sn, and Co) for improving photoactivity compared to the Cu oxide standard are all capable of forming monoxides (CdO, ZnO, SnO, CoO, and NbO) which may allow for easier substitution into CuO, although they form different monoxide crystal structures on their own. CuO forms a monoclinic crystal system, CdO and CoO are cubic, ZnO is most commonly hexagonal (Wurtzite) but also cubic, SnO is tetragonal, and NbO has a cubic structure similar to rock salt.

We synthesized scaled-up films by drop-casting and performed materials characterization to determine if incorporation of these metals altered the crystal structure from that of CuO. The XRD spectra for drop-cast Cu, Cd:Cu = 2:34, Zn:Cu = 3:33, and Sn:Cu = 4:32 oxide films are included in the ESI† (Fig. S1). The strongest peaks for all of these films matched the reference pattern for CuO (PDF#00-048-1548) without any additional peaks for Cd, Zn, or Sn oxides. We also performed UV-vis measurements to determine if incorporation of the metals changed the light absorption of CuO (Fig. S2 in ESI†). The Cu, Cd:Cu = 2:34, Zn:Cu = 3:33, and Sn:Cu = 4:32 oxide films all had similar absorbance. These results suggest that incorporation of Cd, Zn, and Sn (at 11.1% or less metals basis) improves the charge transport and/or photo-reduction kinetics of CuO without modifying the crystal structure or light absorbance.

Similar to the approach used for M–Cu oxide compounds, we compared the most photoactive Bi–M–Cu oxide compounds with the Bi–Cu oxide standard (Bi:Cu = 2:1). 10 out of the 22 elements resulted in a Bi–M–Cu oxide compound with higher photocurrent than the Bi–Cu oxide standard on the same array. Fig. 5 shows a Pareto plot for these photoactive materials.

For the majority of metals the most photoactive Bi–M–Cu oxide did not have a Bi:Cu atomic ratio close to 2:1 (ratio for  $\text{CuBi}_2\text{O}_4$ ). Rather, the combinations with the highest photocurrent contained an excess amount of Cu over Bi (e.g. Bi:Ga:Cu = 7:8:21, Bi:Mo:Cu = 5:4:27, and Bi:Ti:Cu = 3:5:28). In effect these materials were like Bi and M co-doped Cu oxide rather than M doped  $\text{CuBi}_2\text{O}_4$ . However, the three most effective metals (Ag, Cd, Zn) for improving photoactivity over Cu–Bi oxide showed high photoactivity compounds with a Bi:Cu ratio closer to 1:1 (e.g. Bi:Ag:Cu = 1:1:1, Bi:Cd:Cu = 15:2:19, and Bi:Zn:Cu = 14:4:18).

#### 3.2 Cd–Cu oxide results

Because of the effectiveness of Cd at enhancing photoactivity as Cd–Cu and Bi–Cd–Cu oxide it was studied in more detail. Fig. 6 shows the initial  $19 \times 19$  Bi–Cd–Cu array scan, which was carried out in 0.1 M  $\text{Na}_2\text{SO}_4$  (pH 5.9) at  $-0.1$  V vs. Ag/AgCl. The figure shows that 1–6 drops of Cd (5.56–33.3% metals basis) with the remaining drops Cu resulted in higher photocurrents than the Cu oxide standards. It also shows that 1–3 drops of Cd (5.56–16.7% metals basis) in the Bi–Cd–Cu areas of the array had relatively high photocurrent compared to the Cu and Cu–Bi oxide standards. These photoactive areas were used to design the fine increment array and narrow in on the most photoactive

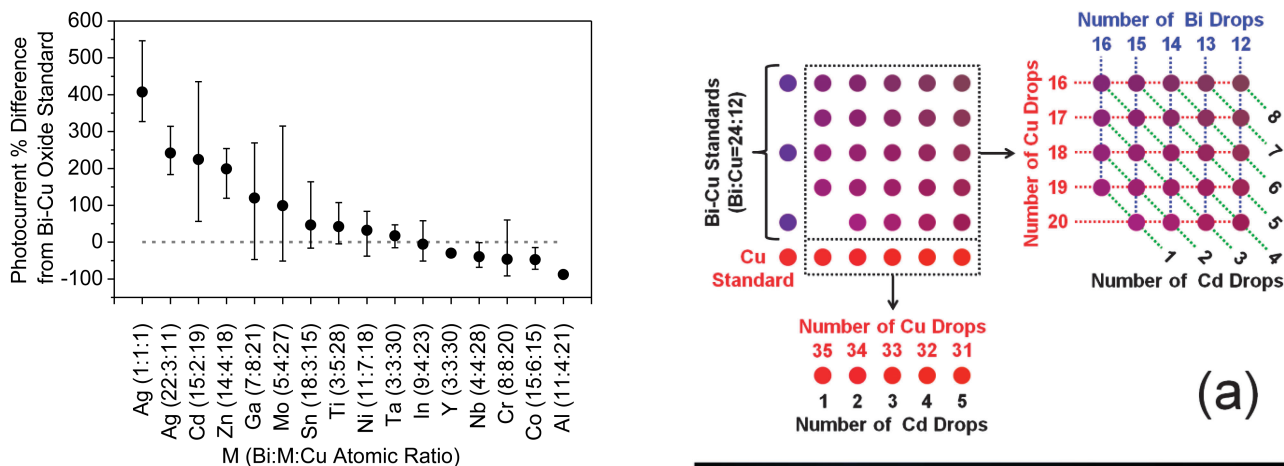


**Fig. 5** Pareto plot of the percent difference in photocurrent of Bi-M-Cu oxide compounds from the Bi-Cu oxide standard. Each point is the average of at least three arrays while the vertical bars are the maximum and minimum. Arrays were scanned in 0.1 M  $\text{Na}_2\text{SO}_4$  (pH 5.9) at a potential of  $-0.1$  V vs. Ag/AgCl (0.45 V vs. RHE).

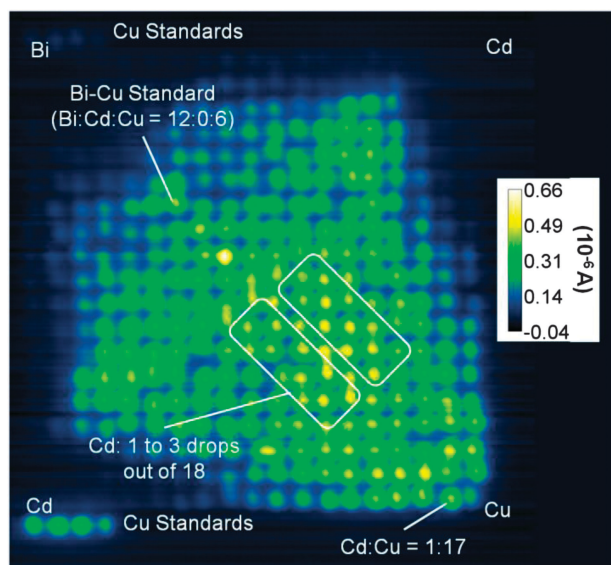


**Fig. 6**  $19 \times 19$  Bi-Cd-Cu array scan results. The spot spacing was  $550 \mu\text{m}$ . The measurement was carried out in 0.1 M  $\text{Na}_2\text{SO}_4$  (pH 5.9) at a potential of  $-0.1$  V vs. Ag/AgCl (0.45 V vs. RHE) with an optical fiber tip scan rate of  $500 \mu\text{m s}^{-1}$ .

Cd : Cu and Bi : Cd : Cu atomic ratios. Fig. 7(a) shows the pattern that was used for the fine increment Bi-Cd-Cu array. The array contained Bi-Cu and Cu oxide standards on the left, a square with Bi-Cd-Cu oxides in the upper right and a row of Cd-Cu oxides on the bottom. Fig. 7(b) shows the scan results for this array. The entire Cd-Cu oxide row had 2–3 times higher photocurrent than the Cu oxide standard and a range of Bi-Cd-Cu oxides with 1–4 drops of Cd (2.78% to 11.1% metals basis) had 1.5–2.5 times higher photocurrent than the Bi-Cu and Cu oxide standards. The optimal atomic ratios of Cd : Cu = 2 : 34 and Bi : Cd : Cu = 15 : 2 : 19 were determined by dispensing and scanning several repeat arrays.

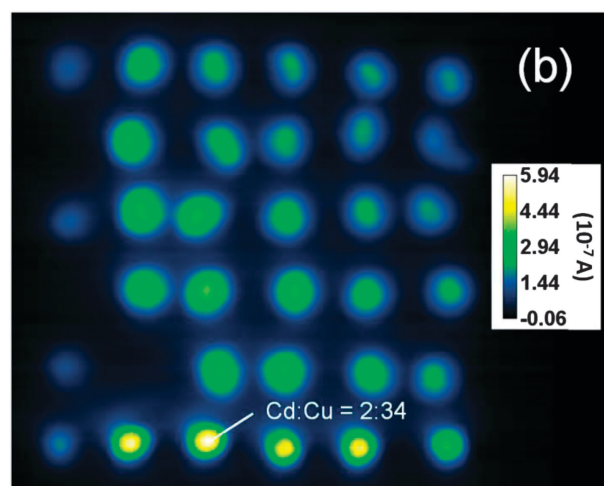


**Fig. 7** Fine increment Bi-Cd-Cu (a) array pattern and (b) scan results. Each spot had a total of 36 drops with a spot spacing was  $1000 \mu\text{m}$ . Scanned at a potential of  $-0.1$  V vs. Ag/AgCl (0.45 V vs. RHE) with an optical fiber tip scan rate of  $250 \mu\text{m s}^{-1}$ .

Scaled-up Cd : Cu = 2 : 34 oxide films synthesized by drop-casting were tested in 0.1 M  $\text{Na}_2\text{SO}_4$  along with 0.1 M phosphate buffer (pH 6.8) to maintain a constant pH. Electrochemical impedance spectroscopy (EIS) was performed to determine the effect of Cd incorporation on the flat band potential ( $V_{\text{FB}}$ ) and carrier donor density ( $N_{\text{D}}$ ). A Mott-Schottky plot for the CuO and Cd : Cu = 2 : 34 oxide film is included in the ESI† (Fig. S3). The line for the CuO film had an  $x$ -axis intercept of  $V_{\text{FB}} \approx 1.24$  V vs. RHE, which is consistent with other reports for CuO in the literature.<sup>14,16</sup> The Cd : Cu = 2 : 34 oxide film had a similar  $x$ -axis intercept ( $V_{\text{FB}} \approx 1.21$  V vs. RHE) but a lower slope indicating a higher  $N_{\text{D}}$  and possibly better conductivity than the CuO film. Fig. 8(a) shows a chopped (dark/white) LSV scan for the CuO and Cd : Cu = 2 : 34 oxide films in 0.1 M  $\text{Na}_2\text{SO}_4$  and 0.1 M phosphate buffer. Consistent with the array scan results, the scaled-up Cd : Cu = 2 : 34 oxide films showed higher photocurrent than CuO.

To test the Cd : Cu = 2 : 34 oxide film stability an illuminated amperometric  $i$ - $t$  measurement was run for several minutes at a constant potential of 0.6 V vs. RHE in buffered electrolyte (see Fig. S4(a) in the ESI†). Regrettably, incorporation of Cd into

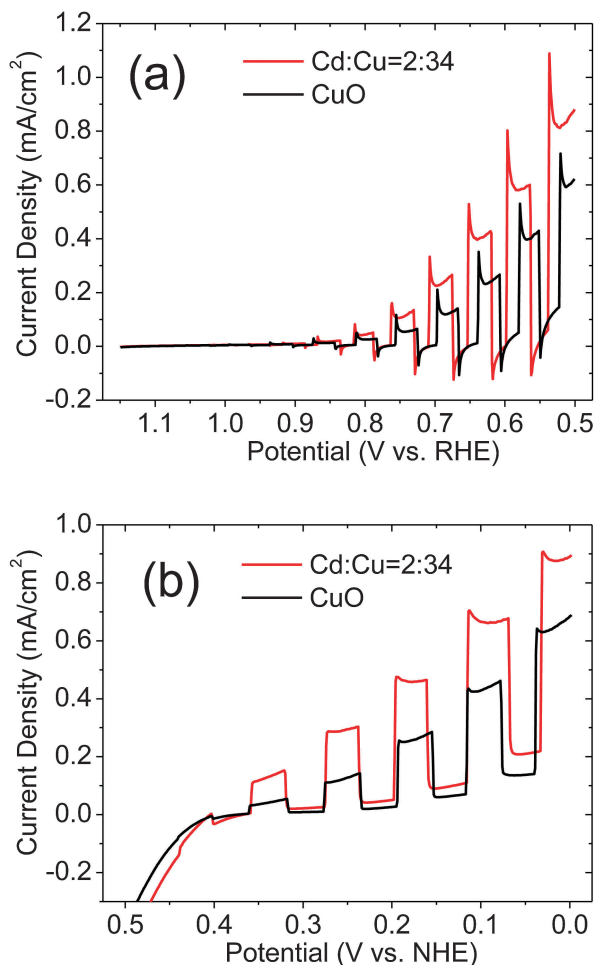


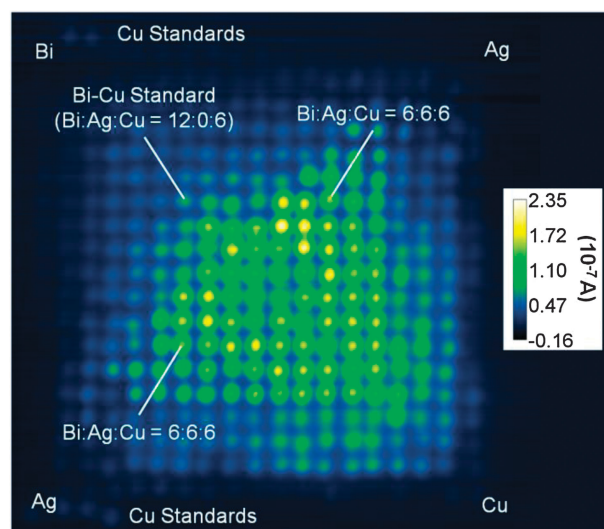
**Fig. 8** Chopped (dark/light) LSV scans for CuO and Cd:Cu = 2:34 oxide films in (a) 0.1 M Na<sub>2</sub>SO<sub>4</sub> and 0.1 M phosphate buffer (pH 6.8) and (b) 10 mM I<sub>2</sub>, 50 mM NaI in acetonitrile. Measurements were done using backside illumination (100 mW cm<sup>-2</sup>) and a scan rate of 0.025 V s<sup>-1</sup>.

CuO did not protect the material from photo-corrosion in the aqueous solution. The photocurrent dropped by about 90% of the initial value after 20 minutes of illumination. The same measurement was conducted for other M-Cu oxide films (Cd:Cu = 2:34, Zn:Cu = 3:33, and Sn:Cu = 4:32) as well and they all showed a large drop in photocurrent. To rule out the presumption that the higher photocurrent of the M-Cu oxide films was merely due to higher photo-corrosion we repeated the PEC tests in a non-aqueous solution containing the iodide/triiodide redox couple. The solution was prepared by dissolving 10 mM I<sub>2</sub> and 50 mM NaI in acetonitrile, which leads to an iodide:triiodide ratio of 4:1.<sup>51</sup> Fig. 8(b) shows a chopped (dark/white) LSV scan for the CuO and Cd:Cu = 2:34 oxide films in this solution with the Cd:Cu = 2:34 oxide film reaching higher photocurrent and also remaining stable. Amperometric *i-t* measurements at 0.2 V vs. NHE were conducted in the iodide-triiodide solution corroborating the improved photoactivity of Cd:Cu = 2:34 oxide over CuO and stability in the non-aqueous electrolyte (see Fig. S4(b) in the ESI†). These results confirm that incorporation of transition and

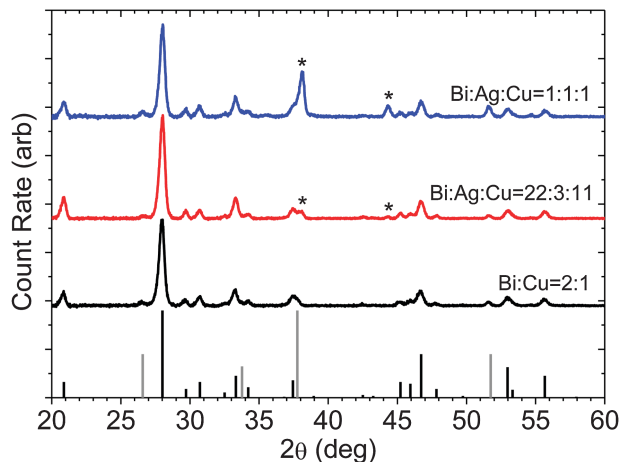
post-transition metals into CuO can improve the performance for photo-reduction reactions. This may be useful if future work leads to methods for stabilizing CuO in aqueous solutions. It has already been demonstrated that Cu<sub>2</sub>O can be protected from photo-corrosion to an extent with nanolayers of Al-doped ZnO and TiO<sub>2</sub>.<sup>52</sup> A similar technique may be effective for CuO based materials.

### 3.3 Bi-Ag-Cu oxide results

Out of the 22 metals tested Ag was certainly the most effective at producing photoactive Bi-M-Cu oxide compounds. Fig. 9 shows the initial 19 × 19 Bi-Ag-Cu array scan with several areas having drastically higher photocurrent than the Bi-Cu and Cu oxide standards, especially for Bi:Ag:Cu atomic ratios near 1:1:1 (6:6:6). Also worth mentioning is that in the Bi-Cu diagonal an excess amount of Cu compared to the Bi-Cu oxide standard (e.g. Bi:Ag:Cu = 10:0:8 compared to Bi:Cu = 12:6) produced a higher photocurrent. Similarly, for the Bi-Cd-Cu array results in Fig. 6, the Bi:Cu:Cu = 10:0:8 spot shows more photocurrent than the Bi-Cu oxide standard. Initially this led us to prepare scaled-up Bi-M-Cu oxide films with excess Cu by drop-casting. However, PEC measurements of the films with excess Cu (e.g. Bi:Ag:Cu = 1:1:1, Bi:Cu:Cu = 15:2:19, and Bi:Zn:Cu = 14:4:18) tended to show more dark current and less long-term stability than films synthesized with a Bi:Cu atomic ratio closer to 2:1. In addition the excess Cu did not result in any new compounds other than CuBi<sub>2</sub>O<sub>4</sub>, which is apparent from XRD measurements. Fig. 10 shows the XRD spectra for films synthesized by drop-casting with atomic ratios of Bi:Cu = 2:1, Bi:Ag:Cu = 22:3:11, and Bi:Ag:Cu = 1:1:1. Even when excess Cu was added, as in the case of Bi:Ag:Cu = 1:1:1, the largest XRD peaks matched the reference pattern for kusachiite, CuBi<sub>2</sub>O<sub>4</sub> (PDF# 00-042-0334) which has a Bi:Cu ratio of 2:1 and there were no additional peaks related to a



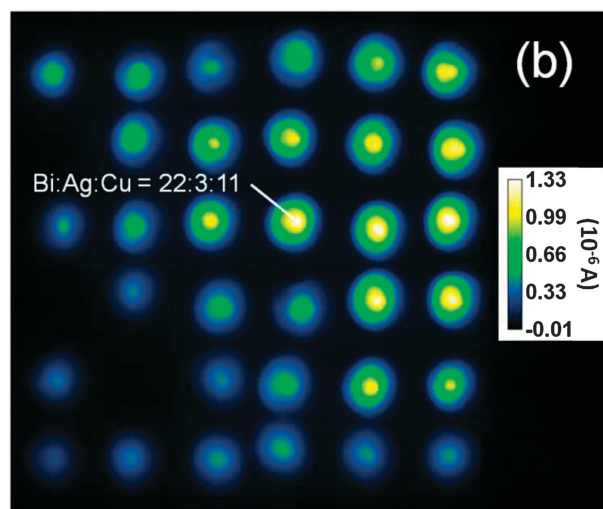
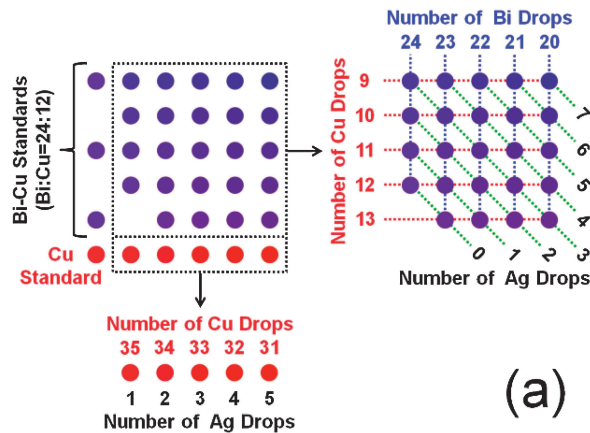
**Fig. 9** 19 × 19 Bi-Ag-Cu array scan results. The spot spacing was 550 μm. The measurement was carried out in 0.1 M Na<sub>2</sub>SO<sub>4</sub> (pH 5.9) at a potential of -0.1 V vs. Ag/AgCl (0.45 V vs. RHE) with an optical fiber tip scan rate of 500 μm s<sup>-1</sup>.



**Fig. 10** XRD spectra for bulk films drop-cast with atomic ratios of Bi:Cu = 2:1, Bi:Ag:Cu = 22:3:11, and Bi:Ag:Cu = 1:1:1. Grey vertical lines (I) represent the cassiterite, SnO<sub>2</sub> reference pattern (PDF# 00-042-0334). Black vertical lines (II) represent the kusachiite, CuBi<sub>2</sub>O<sub>4</sub> reference pattern (PDF# 00-042-0334). Asterisks (\*) indicate the silver, Ag(111) and (200) peaks at  $2\theta$  values of 38.1° and 44.3°, respectively (PDF#00-004-0783).

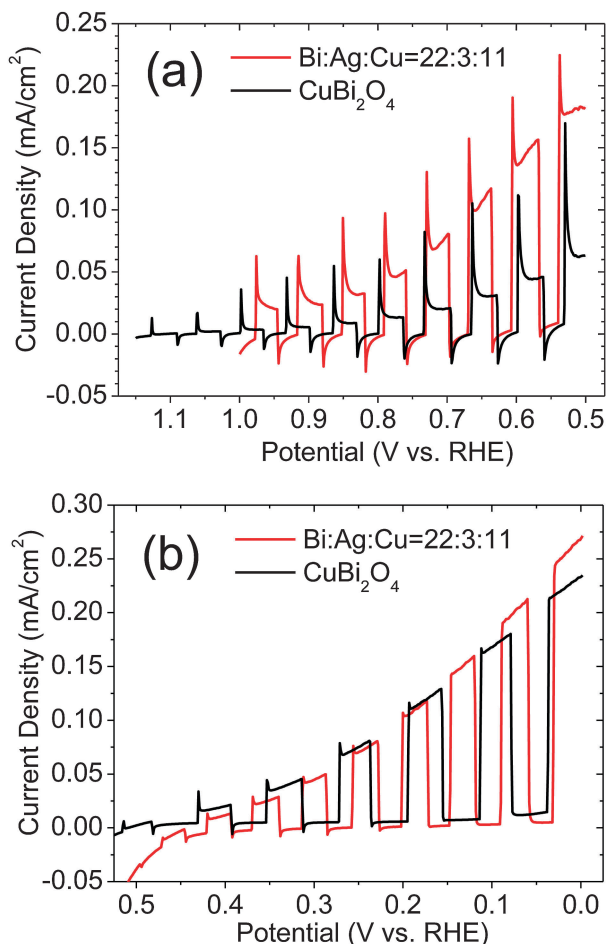
Cu compound. This suggests that the excess Cu is incorporated into the interstitial sites of CuBi<sub>2</sub>O<sub>4</sub>, which may contribute to the instability during PEC measurements. Previously we showed that BiVO<sub>4</sub> films synthesized with excess V (Bi:V = 1:2) had much higher initial photocurrents than BiVO<sub>4</sub> synthesized with stoichiometric Bi and V (Bi:V = 1:1); however, much of the initial photocurrent was due to photo-corrosion and dissolution of excess V into solution.<sup>53</sup> For this reason we focused on materials characterization and PEC testing of scaled-up films with a Bi:Cu atomic ratio of 2:1 (e.g. CuBi<sub>2</sub>O<sub>4</sub> and Bi:Ag:Cu = 22:3:11). Interestingly, Ag was not incorporated into CuBi<sub>2</sub>O<sub>4</sub> as an oxide but rather segregated primarily as reduced Ag. The XRD patterns for both Bi:Ag:Cu = 22:3:11 and Bi:Ag:Cu = 1:1:1 showed the emergence of peaks at  $2\theta$  values of 38.1° and 44.3° corresponding to the (111) and (200) peaks in the reference pattern for Ag (PDF#00-004-0783). Incorporation of Ag did not result any shifting of the CuBi<sub>2</sub>O<sub>4</sub> peaks.

Fig. 11(a) shows the fine increment Bi–Ag–Cu array pattern and Fig. 11(b) shows the array scan results for this pattern. The fine increment array scans demonstrated that a range of Ag concentrations (8.3% to 19.4% metals basis) improved the photocurrent compared to CuBi<sub>2</sub>O<sub>4</sub>. After dispensing and scanning several different arrays the optimal Bi:Ag:Cu atomic ratio was determined to be 22:3:11 (8.3% Ag metals basis), which consistently showed 2.5 times higher photocurrent than CuBi<sub>2</sub>O<sub>4</sub>. The improvement in photocurrent of Bi:Ag:Cu = 22:3:11 oxide films over CuBi<sub>2</sub>O<sub>4</sub> was confirmed by PEC testing of scaled-up films. Fig. 12(a) shows the chopped (dark/white) LSV scan for these films in 0.1 M Na<sub>2</sub>SO<sub>4</sub> and 0.1 M phosphate buffer. At 0.6 V vs. RHE the photocurrent for the Bi:Ag:Cu = 22:3:11 oxide film was about 4 times higher than that of CuBi<sub>2</sub>O<sub>4</sub>. In addition the CuBi<sub>2</sub>O<sub>4</sub> film showed significantly larger transient spikes in the photocurrent traces. For n-type semiconductors large anodic and cathodic spikes are



**Fig. 11** Fine increment Bi–Ag–Cu (a) array pattern and (b) scan results. Each spot had a total of 36 drops with a spot spacing was 1000  $\mu\text{m}$ . Scanned at a potential of  $-0.1$  V vs. Ag/AgCl (0.45 V vs. RHE) with an optical fiber tip scan rate of 250  $\mu\text{m s}^{-1}$ .

often attributed to recombination or back reactions of the photo-generated species on the surface of the semiconductor.<sup>17,54,55</sup> The large transient spikes imply that the CuBi<sub>2</sub>O<sub>4</sub> surface has slower reaction kinetics for the photo-reduction reaction. To further assess differences in kinetics we tested the CuBi<sub>2</sub>O<sub>4</sub> and Bi:Ag:Cu = 22:3:11 oxide films in the non-aqueous iodide–triiodide electrolyte prepared from 10 mM I<sub>2</sub> and 50 mM NaI, in acetonitrile. The triiodide species is expected to undergo a fast reduction lessening the influence of reaction kinetics on the overall photoactivity. Fig. 12(b) shows the chopped (dark/light) LSV scans. In the iodide–triiodide electrolyte the CuBi<sub>2</sub>O<sub>4</sub> and Bi:Ag:Cu = 22:3:11 oxide films had very similar photo-currents without significant transient spikes. The relative differences in photocurrents for CuBi<sub>2</sub>O<sub>4</sub> and Bi:Ag:Cu = 22:3:11 oxide in the aqueous and iodide–triiodide electrolytes confirm that Bi:Ag:Cu = 22:3:11 oxide has better reaction kinetics for the photo-reduction reactions in the aqueous solution, which likely includes H<sup>+</sup> reduction. Ag is not regarded as an effective electrocatalyst for HER, but computational studies have suggested that surface alloys can be much more active for HER than the individual elements from



**Fig. 12** Chopped (dark/light) LSV scans for  $\text{CuBi}_2\text{O}_4$  and  $\text{Bi:Ag:Cu} = 22:3:11$  oxide films synthesized by drop-cast in (a) 0.1 M  $\text{Na}_2\text{SO}_4$  and 0.1 M phosphate buffer (pH 6.8) and (b) 10 mM  $\text{I}_2$ , 50 mM  $\text{NaI}$  in acetonitrile. Measurements were done using backside illumination ( $100 \text{ mW cm}^{-2}$ ) and a scan rate of  $0.025 \text{ V s}^{-1}$ .

which the alloys are composed.<sup>56</sup> We also tested  $\text{Bi:Ag:Cu} = 22:3:11$  oxide films with Pt electrodeposited on the surface. This increased the dark current but did not significantly increase the photocurrent for chopped LSV scans in electrolyte that had not been purged with an inert gas (see Fig. S5(a) in the ESI†).

To uncover more reasons that Ag incorporation improved the photocurrent of  $\text{CuBi}_2\text{O}_4$  we performed materials characterization of the scaled-up films. UV-vis measurements showed that Ag incorporation did not change the absorption significantly (see Fig. S6 in the ESI†). SEM images revealed slight differences in surface structures and morphologies for  $\text{CuBi}_2\text{O}_4$  and  $\text{Bi:Ag:Cu} = 22:3:11$  oxide films. Fig. 13 shows high and low magnification SEM images of the  $\text{CuBi}_2\text{O}_4$  and  $\text{Bi:Ag:Cu} = 22:3:11$  spots in a fine detail array and SEM images of the drop-cast films are included in the ESI† (Fig. S7). The images show that the  $\text{Bi:Ag:Cu} = 22:3:11$  oxide contains a mix of larger features (50–250 nm coalesced particles) and much smaller particles (<10 nm diameter) while the  $\text{CuBi}_2\text{O}_4$  contained a more dense layer with less variation in feature sizes (<100 nm coalesced particles). The larger features of the  $\text{Bi:Ag:Cu} = 22:3:11$  oxide may improve charge transport through the film

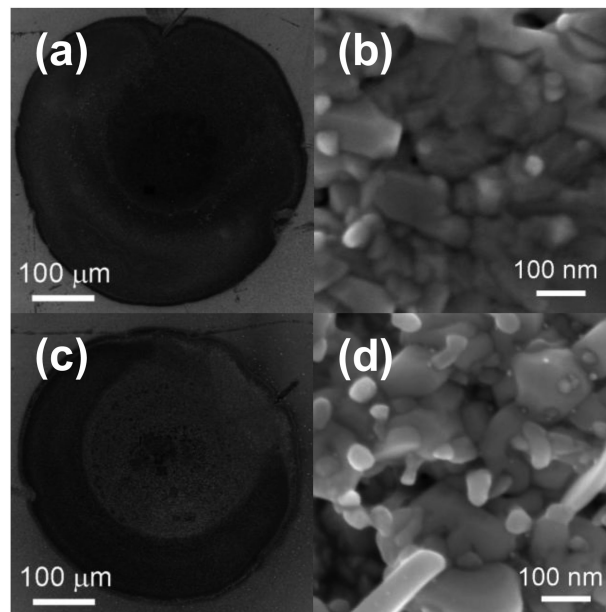


**Fig. 13** SEM images of a fine detail  $\text{Bi-Ag-Cu}$  array. (a) Entire  $\text{Bi:Cu} = 2:1$  spot, (b) area in centre of  $\text{Bi:Cu} = 2:1$  spot, (c) entire  $\text{Bi:Ag:Cu} = 22:3:11$  spot, and (d) area in centre of  $\text{Bi:Ag:Cu} = 22:3:11$  spot.

while the smaller particles on the surface might act as reaction sites to improve the kinetics of the surface reaction.

Both EDS and XPS were used to analyze the chemical composition of the  $\text{CuBi}_2\text{O}_4$  and  $\text{Bi:Ag:Cu} = 22:3:11$  oxide films. EDS mapping of a  $\text{Bi-Ag-Cu}$  array spot showed that Bi, Ag, and Cu were distributed throughout the entire spot and quantification of the EDS spectra from several spots confirmed that the dispensed atomic ratios were within  $\pm 1$  drop of the expected values. The EDS data is included in the ESI† (Fig. S8 and Table S1). Fig. 14 shows the XPS spectra for scaled-up  $\text{CuBi}_2\text{O}_4$  and  $\text{Bi:Ag:Cu} = 22:3:11$  oxide films. The Bi 4f, Cu 2p, and O 1s regions were similar for both compositions with the main Bi 4f 7/2, Cu 2p 3/2, and O 1s peaks at 158.4 eV, 934.0 eV, and 529.3 eV, respectively. This corresponds to oxidation states of  $\text{Bi}^{3+}$ ,  $\text{Cu}^{2+}$ , and  $\text{O}^{2-}$  and matches the stoichiometry of the films.<sup>57</sup> As mentioned previously, Ag appeared to be incorporated in the reduced form based on XRD measurements. The XPS spectra for the  $\text{Bi:Ag:Cu} = 22:3:11$  oxide film showed a Ag 3d 5/2 peak at 368.1 eV, which is in range of the experimentally reported binding energies for pure Ag at 368.0–368.4 eV.<sup>57–59</sup> But distinguishing the oxidation state of Ag by XPS is a challenge because the reported binding energies of  $\text{Ag}_2\text{O}$  and AgO overlap at 367.6–368.4 eV and 367.2–368.1 eV, respectively.<sup>57,58</sup> As further proof that Ag is incorporated in the reduced form we ran CV scans in the dark on the films between 0.6 to 1.3 V vs. RHE (Fig. S10 in the ESI†). The CV scan for the  $\text{CuBi}_2\text{O}_4$  film was perfectly flat while that for  $\text{Bi:Ag:Cu} = 22:3:11$  oxide showed a large anodic spike for the oxidation of Ag when scanning more positive than 1.0 V vs. RHE. Ag metal is known for exceptionally low contact resistance and very high electrical conductivity while Ag oxides have relatively low conductivity.<sup>58,60</sup> Incorporation of reduced Ag into  $\text{CuBi}_2\text{O}_4$  likely improves the conductivity and charge transport through the film,

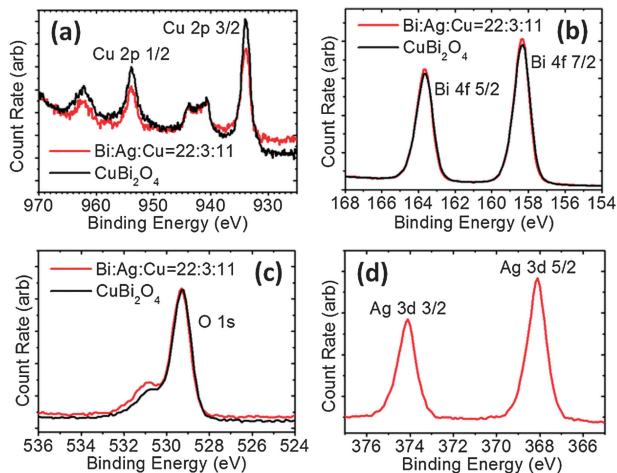


**Fig. 14** XPS spectra for  $\text{CuBi}_2\text{O}_4$  and Bi:Ag:Cu = 22:3:11 oxide films. (a) Cu 2p (b) Bi 4f (c) O 1s and (d) Ag 3d regions.

which is another possible reason for the improvement in photoactivity. The improvement may also be related spectral sensitization by surface plasmon resonance of dispersed Ag nanoparticles. This was proposed for a study in which 50% Ag incorporation into  $\text{Fe}_2\text{O}_3$  resulted in 5 nm Ag nanoparticles that were observed by transmission electron microscopy (TEM).<sup>61</sup>

Because the Ag in the Bi:Ag:Cu = 22:3:11 oxide films were easily oxidized at potentials more positive than 1.0 V vs. RHE the films were kept between 0.5 and 1.0 V vs. RHE during PEC testing. Within this range both  $\text{CuBi}_2\text{O}_4$  and Bi:Ag:Cu = 22:3:11 oxide films appeared to be relatively stable in neutral aqueous electrolyte. Long-term PEC testing was also performed. Fig. 15 shows the illuminated amperometric *i-t* measurement for  $\text{CuBi}_2\text{O}_4$  and Bi:Ag:Cu = 22:3:11 oxide films and a Bi:Ag:Cu = 22:3:11 oxide film with Pt electrodeposited on the surface. Initially the films showed a drop in photocurrent, but afterwards the photocurrents remained fairly constant for 45 minutes. As mentioned previously, Pt did not improve the photocurrent significantly for chopped LSV scans, but as shown in Fig. 15 it did enhance the photocurrent for long-term testing at a constant potential.

Unless otherwise indicated the PEC testing of scaled-up films was done without purging the electrolyte with an inert gas so a portion of the photocurrent came from the reduction of species other than  $\text{H}^+$ . When the electrolyte was purged with an inert gas such as Ar or  $\text{N}_2$  the photocurrent was lower, even with the addition of Pt. This is seen by comparing Fig. S5(a) and S5(b) in the ESI.† To confirm that the films were actually capable of reducing  $\text{H}^+$  and evolving  $\text{H}_2$  we performed qualitative  $\text{H}_2$  detection measurements for Bi:Ag:Cu = 22:3:11 oxide films with and without Pt deposited on the surface. The films were placed in a sealed PEC cell with 0.1 M  $\text{Na}_2\text{SO}_4$  and 0.1 M phosphate buffer (pH 6.8) that had been purged with Ar for 30 minutes. Then the films were held at a constant potential of 0.6 V vs. RHE and illuminated with a 100 W Xe lamp for about 5 hours. We observed formation of small ( $\sim 1$  mm) bubbles on the films with and without Pt on the surface. The gas above the

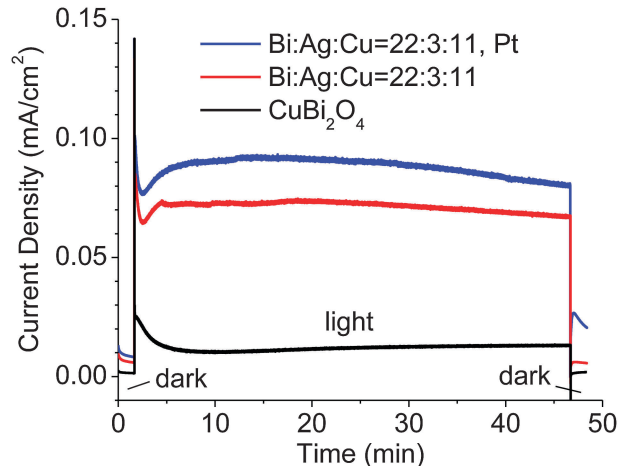


**Fig. 15** Amperometric *i-t* curve for  $\text{CuBi}_2\text{O}_4$  and Bi:Ag:Cu = 22:3:11 oxide films. Measurements done in 0.1 M  $\text{Na}_2\text{SO}_4$  and 0.1 M phosphate buffer solution (pH 6.8) at constant potential of 0.6 V vs. RHE.

electrolyte was collected and measured by GC. A significant amount of  $\text{H}_2$  was detected for the film with Pt but not for the film without Pt. Since 0.6 V vs. RHE is well positive of the thermodynamic  $\text{H}^+$  reduction potential, the  $\text{H}_2$  must have been produced photoelectrochemically.

## 4. Conclusions

We have designed a new array dispenser and scanner system for materials research by combinatorial chemistry. The system was used to study the incorporation of 22 different transition and post-transition metals (M) into  $\text{CuO}$  and  $\text{CuBi}_2\text{O}_4$  to improve the PEC performance for photo-reduction reactions including hydrogen evolution. We identified 10 metals that produced M-Cu oxide compounds with higher photoactivity than  $\text{CuO}$ . The most photoactive M-Cu oxide materials contained 2.78 to 11.1% M incorporated into  $\text{CuO}$  (metals basis). Cd, Zn, and Sn were the most effective at improving the photocurrent of  $\text{CuO}$  and with optimal atomic ratios of Cd:Cu = 2:34, Zn:Cu = 3:33, and Sn:Cu = 4:32. Unfortunately incorporation of these elements into  $\text{CuO}$  did not prevent photo-corrosion in aqueous solutions, but it did enhance the photocurrent with stability in non-aqueous iodide-triiodide solutions. For Bi-M-Cu oxides we found 10 metals that increased the photocurrent relative to  $\text{CuBi}_2\text{O}_4$ . Ag was the most effective element at improving the photoactivity of  $\text{CuBi}_2\text{O}_4$  while also maintaining the stability in neutral electrolyte solutions. Films with a Bi:Ag:Cu atomic ratio of 22:3:11 produced photocurrents up to 5 times higher than  $\text{CuBi}_2\text{O}_4$  between 1.0 and 0.5 V vs. RHE, which is a reasonable operating range for a tandem PEC cell. With the addition of a HER electrocatalyst such as Pt, these films were capable of evolving hydrogen under illumination in a neutral electrolyte solution at a potential of 0.6 V vs. RHE.

## Acknowledgements

The authors gratefully acknowledge the Division of Chemical Sciences, Geosciences, and Biosciences, Office of Basic Energy

Sciences of the U.S. Department of Energy through Grant DE-FG02-09ER16119, and the Welch Foundation (C.B.M. for Grant F-1436 and A.J.B. for Grant F-0021) for funding this work. Additionally we acknowledge the National Science Foundation (Grant No. 0618242) which funded the X-ray Photoelectron Spectrometer used for these studies. We would like to thank Mark Ramsdale (Ramsdale Software) for assistance in writing the LabVIEW program to control the evaporators. S.P. Berglund thanks the National Science Foundation Graduate Research Fellowship Program for financial support and the University of Texas at Austin Cockrell School of Engineering for the Thrust 2000 Graduate Fellowship in Engineering (Harry P. Whitworth endowed). P. D. Núñez acknowledges the National Science Foundation (Grant No. CHE-1003947) for support as a summer 2011 undergraduate REU student.

## References

- 1 R. van de Krol and M. Grätzel, *Photoelectrochemical Hydrogen Production*, Springer, New York, Dordrecht, Heidelberg, London, 2012.
- 2 M. F. Weber and M. J. Dignam, *Int. J. Hydrogen Energy*, 1986, **11**, 225–232.
- 3 J. R. Bolton, S. J. Strickler and J. S. Connolly, *Nature*, 1985, **316**, 495–500.
- 4 M. G. Walter, E. L. Warren, J. R. McKone, S. W. Boettcher, Q. Mi, E. A. Santori and N. S. Lewis, *Chem. Rev.*, 2011, **111**, 5815.
- 5 E. Aharon-Shalom and A. Heller, *J. Electrochem. Soc.*, 1982, **129**, 2865–2866.
- 6 Y. Nakato, S. Tonomura and H. Tsubomura, *Ber. Bunsen-Ges.*, 1976, **80**, 1289–1293.
- 7 R. N. Dominey, N. S. Lewis, J. A. Bruce, D. C. Bookbinder and M. S. Wrighton, *J. Am. Chem. Soc.*, 1982, **104**, 467–482.
- 8 Y. Nakato, H. Yano, S. Nishiura, T. Ueda and H. Tsubomura, *J. Electroanal. Chem. Interfacial Electrochem.*, 1987, **228**, 97–108.
- 9 J. Oh, T. G. Deutsch, H.-C. Yuan and H. M. Branz, *Energy Environ. Sci.*, 2011, **4**, 1690–1694.
- 10 B. Marsen, B. Cole and E. L. Miller, *Sol. Energy Mater. Sol. Cells*, 2008, **92**, 1054–1058.
- 11 D. Yokoyama, T. Minegishi, K. Maeda, M. Katayama, J. Kubota, A. Yamada, M. Konagai and K. Domen, *Electrochem. Commun.*, 2010, **12**, 851–853.
- 12 K. Nakaoka, J. Ueyama and K. Ogura, *J. Electrochem. Soc.*, 2004, **151**, C661–C665.
- 13 J. Ghijsen, L. H. Tjeng, J. van Elp, H. Eskes, J. Westerink, G. A. Sawatzky and M. T. Czyzyk, *Phys. Rev. B: Condens. Matter Mater. Phys.*, 1988, **38**, 11322–11330.
- 14 F. P. Koffyberg and F. A. Benko, *J. Appl. Phys.*, 1982, **53**, 1173–1177.
- 15 Y. S. Chaudhary, A. Agrawal, R. Shrivastav, V. R. Satsangi and S. Dass, *Int. J. Hydrogen Energy*, 2004, **29**, 131–134.
- 16 D. Chauhan, V. R. Satsangi, S. Dass and R. Shrivastav, *Bull. Mater. Sci.*, 2006, **29**, 709–716.
- 17 K. L. Hardee and A. J. Bard, *J. Electrochem. Soc.*, 1977, **124**, 215–224.
- 18 H. Gerischer, *J. Electroanal. Chem. Interfacial Electrochem.*, 1977, **82**, 133–143.
- 19 T. Arai, Y. Konishi, Y. Iwasaki, H. Sugihara and K. Sayama, *J. Comb. Chem.*, 2007, **9**, 574–581.
- 20 N. T. Hahn, V. C. Holmberg, B. A. Korgel and C. B. Mullins, *J. Phys. Chem. C*, 2012, **116**, 6459–6466.
- 21 Z. Zou, J. Ye, K. Sayama and H. Arakawa, *Nature*, 2001, **414**, 625–627.
- 22 R. Asahi, T. Morikawa, T. Ohwaki, K. Aoki and Y. Taga, *Science*, 2001, **293**, 269–271.
- 23 M. Woodhouse and B. A. Parkinson, *Chem. Mater.*, 2008, **20**, 2495–2502.
- 24 X. Chen, S. Shen, L. Guo and S. S. Mao, *Chem. Rev.*, 2010, **110**, 6503–6570.
- 25 R. B. Merrifield, *Science*, 1965, **150**, 178–185.
- 26 M. A. Gallop, R. W. Barrett, W. J. Dower, S. P. A. Fodor and E. M. Gordon, *J. Med. Chem.*, 1994, **37**, 1233–1251.
- 27 G. Briceño, H. Chang, X. Sun, P. G. Schultz and X. D. Xiang, *Science*, 1995, **270**, 273–275.
- 28 E. Danielson, J. H. Golden, E. W. McFarland, C. M. Reaves, W. H. Weinberg and X. D. Wu, *Nature*, 1997, **389**, 944–948.
- 29 S. M. Senkan, *Nature*, 1998, **394**, 350–353.
- 30 B. Jandeleit, D. J. Schaefer, T. S. Powers, H. W. Turner and W. H. Weinberg, *Angew. Chem., Int. Ed.*, 1999, **38**, 2494–2532.
- 31 J. C. Meredith, A. P. Smith, A. Karim and E. J. Amis, *Macromolecules*, 2000, **33**, 9747–9756.
- 32 W. F. Maier, K. Stöwe and S. Sieg, *Angew. Chem., Int. Ed.*, 2007, **46**, 6016–6067.
- 33 C. Lettmann, H. Hinrichs and W. F. Maier, *Angew. Chem., Int. Ed.*, 2001, **40**, 3160–3164.
- 34 A. Nakayama, E. Suzuki and T. Ohmori, *Appl. Surf. Sci.*, 2002, **189**, 260–264.
- 35 T. F. Jaramillo, S.-H. Baeck, A. Kleiman-Shwarsstein and E. W. McFarland, *Macromol. Rapid Commun.*, 2004, **25**, 297–301.
- 36 T. F. Jaramillo, S.-H. Baeck, A. Kleiman-Shwarsstein, K.-S. Choi, G. D. Stucky and E. W. McFarland, *J. Comb. Chem.*, 2004, **7**, 264–271.
- 37 J. I. Goldsmith, W. R. Hudson, M. S. Lowry, T. H. Anderson and S. Bernhard, *J. Am. Chem. Soc.*, 2005, **127**, 7502–7510.
- 38 Q. X. Dai, H. Y. Xiao, W. S. Li, Y. Q. Na and X. P. Zhou, *Appl. Catal., A*, 2005, **290**, 25–35.
- 39 M. Seyler, K. Stoewe and W. F. Maier, *Appl. Catal., B*, 2007, **76**, 146–157.
- 40 M. Woodhouse, G. S. Herman and B. A. Parkinson, *Chem. Mater.*, 2005, **17**, 4318–4324.
- 41 J. E. Katz, T. R. Gingrich, E. A. Santori and N. S. Lewis, *Energy Environ. Sci.*, 2009, **2**, 103–112.
- 42 J. Lee, H. Ye, S. Pan and A. J. Bard, *Anal. Chem.*, 2008, **80**, 7445–7450.
- 43 J. S. Jang, J. Lee, H. Ye, F.-R. F. Fan and A. J. Bard, *J. Phys. Chem. C*, 2009, **113**, 6719–6724.
- 44 H. Ye, J. Lee, J. S. Jang and A. J. Bard, *J. Phys. Chem. C*, 2010, **114**, 13322–13328.

- 45 H. S. Park, K. E. Kweon, H. Ye, E. Paek, G. S. Hwang and A. J. Bard, *J. Phys. Chem. C*, 2011, **115**, 17870–17879.
- 46 N. T. Hahn and C. B. Mullins, *Chem. Mater.*, 2010, **22**, 6474–6482.
- 47 S. P. Berglund, A. J. E. Rettie, S. Hoang and C. B. Mullins, *Phys. Chem. Chem. Phys.*, 2012, **14**, 7065–7075.
- 48 M. Trari, A. Bouguelia and Y. Bessekhoud, *Sol. Energy Mater. Sol. Cells*, 2006, **90**, 190–202.
- 49 S. Saadi, A. Bouguelia and M. Trari, *Renewable Energy*, 2006, **31**, 2245–2256.
- 50 G. K. Mor, O. K. Varghese, R. H. T. Wilke, S. Sharma, K. Shankar, T. J. Latempa, K.-S. Choi and C. A. Grimes, *Nano Lett.*, 2008, **8**, 1906–1911.
- 51 V. A. Macagno, M. C. Giordano and A. J. Arvía, *Electrochim. Acta*, 1969, **14**, 335–357.
- 52 A. Paracchino, V. Laporte, K. Sivula, M. Grätzel and E. Thimsen, *Nat. Mater.*, 2011, **10**, 456–461.
- 53 S. P. Berglund, D. W. Flaherty, N. T. Hahn, A. J. Bard and C. B. Mullins, *J. Phys. Chem. C*, 2010, **115**, 3794–3802.
- 54 P. Iwanski, J. S. Curran, W. Gissler and R. Memming, *J. Electrochem. Soc.*, 1981, **128**, 2128–2133.
- 55 M. Anderman and J. H. Kennedy, *J. Electrochem. Soc.*, 1984, **131**, 21–26.
- 56 J. Greeley, T. F. Jaramillo, J. Bonde, I. Chorkendorff and J. K. Nørskov, *Nat. Mater.*, 2006, **5**, 909–913.
- 57 C. D. Wagner, A. V. Naumkin, A. Kraut-Vass, J. W. Allison, C. J. Powell and J. R. Rumble, *NIST X-ray Photoelectron Spectroscopy Database, Version 3.5*, National Institute of Standards and Technology, Gaithersburg, August 15, 2007.
- 58 S. B. Rivers, G. Bernhardt, M. W. Wright, D. J. Frankel, M. M. Steeves and R. J. Lad, *Thin Solid Films*, 2007, **515**, 8684–8688.
- 59 A. Barrie and N. E. Christensen, *Phys. Rev. B: Condens. Matter Mater. Phys.*, 1976, **14**, 2442–2447.
- 60 D. R. Smith and F. R. Fickett, *J. Res. Natl. Inst. Stand. Technol.*, 1995, **100**, 119–171.
- 61 J. S. Jang, K. Y. Yoon, X. Xiao, F.-R. F. Fan and A. J. Bard, *Chem. Mater.*, 2009, **21**, 4803–4810.